Driving Forces for Limited Tectonics on Venus

David T. Sandwell

Scripps Institution of Oceanography, La Jolla, California 92093–0225
E-mail: sandwell@radar.ucsd.edu

Catherine L. Johnson

Carnegie Institution of Washington, 5241 Broad Branch Rd. NW, Washington, DC 20015

Frank Bilotti

Princeton University, Guyot Hall, Princeton, New Jersey 08544

and

John Suppe

Princeton University, Guyot Hall, Princeton, New Jersey 08544

The very high correlation of geoid height and topography on Venus, along with the high geoid topography ratio, can be interpreted as local isostatic compensation and/or dynamic compensation of topography at depths ranging from 50 to 350 km. For local compensation within the lithosphere, the swell-push force is proportional to the first moment of the anomalous density. Since the long-wavelength isostatic geoid height is also proportional to the first moment of the anomalous density, the swell push force is equal to the geoid height scaled by $-g^2/2\pi G$. Because of this direct relationship, the style (i.e., thermal, Airy, or Pratt compensation) and depth of compensation do not need to be specified and can in fact vary over the surface. Phillips (1990) showed that this simple relationship between swell-push force and geoid also holds for dynamic uplift by shear traction on the base of the lithosphere caused by thermal convection of an isoviscous, infinite half-space mantle. Thus for all reasonable isostatic models and particular classes of dynamic models, the geoid height uniquely determines the magnitude of the swell-push body force that is applied to the venusian lithosphere.

Given this body force and assuming Venus can be approximated by a uniform thickness thin elastic shell over an inviscid sphere, we calculate the present-day global strain field using equations given in Banerdt (1986); areas of positive geoid height are in a state of extension while areas of negative geoid height are in a state of compression. The present-day model strain field is compared to global strain patterns inferred from Magellan-derived maps of wrinkle ridges and rift zones. Wrinkle ridges, which are believed to reflect distributed compressive deformation, are generally confined to regions with geoid of less than 20 m while rift zones are found primarily along geoid highs. Moreover, much of the observed deformation matches the present-day model strain orientations suggesting that most of the rifts on Venus and many of the wrinkle ridges formed in a stress field similar to the present one. In several large regions, the present-day model strain pattern does not match the observations. This suggests that either the geoid has changed significantly since most of the strain occurred or our model assumptions are incorrect (e.g., there could be local plate boundaries where the stress pattern is discontinuous). Since the venusian lithosphere shows evidence for limited strain, the calculation also provides an estimate of the overall strength of the lithosphere in compression and extension which can be compared with rheological models of yield strength versus depth. At the crests of the major swells, where evidence for rifting is abundant, we find that the temperature gradient must be at least 7 K/km. © 1997 Academic Press

INTRODUCTION

Unlike on Earth, geoid height and topography are almost perfectly correlated on Venus (Phillips and Lambeck 1980, Sjogren *et al.* 1983, Smrekar and Phillips 1991, Simons *et al.* 1994, Bills and Lemoine 1995), especially at long wavelengths. Since the interior of Venus must behave as a fluid on geological time scales, the long-wavelength topography is probably locally compensated by buoyancy forces (static or dynamic) directly beneath the load. The absence of large-scale plate motions and plate boundaries

(Solomon *et al.* 1992), coupled with the inferred high strength of the venusian lithosphere from flexural studies (Sandwell and Schubert 1992a, Johnson and Sandwell 1994, Phillips 1994, Brown and Grimm 1996) and the inferred high crustal strength due to the lack of water (Oyama *et al.* 1980, Mackwell *et al.* 1995), implies that stresses can be transmitted over global distances; studies of wrinkle ridge patterns are consistent with this hypothesis (Bilotti and Suppe 1995, Grofils and Head 1994).

Approximating the venusian lithosphere by a continuous elastic shell leads to a nearly unique estimate of the present-day global strain field in the lithosphere. To demonstrate this, we first equate the swell-push body force in the lithosphere to the geoid height without making assumptions about the depth or mode of compensation. Given this swell-push body force and the assumption of a uniform-thickness thin elastic lithosphere, we calculate the mean strain in an elastic sheet (Cartesian coordinates). Then we use the solution given in Banerdt (1986) to correct the flat-Earth solution for the more realistic spherical shell case. We compare model horizontal strains to global maps of rift zones (Coburn 1993) and wrinkle ridges (Bilotti and Suppe 1995). Finally, we compare the stress integrated over the plate thickness to the integrated strength obtained from realistic yield-strength envelope models to place bounds on the lithospheric temperature gradient.

While our analysis is based almost entirely on previously published models, these models are combined to minimize the number of assumptions and unknown parameters. Parsons and Richter (1980) and Dahlen (1981) showed that for lithospheric cooling on the Earth, the swell-push force is equal to geoid height times $-g^2/2\pi G$. Fleitout and Frio-devaux (1982, 1983) and Crough (1983) extended this idea to show that this relationship holds for all types of local compensation including Airy and Pratt. Moreover, Crough (1983) discussed the implied state of compressional stress in the deep ocean basins and shows that thermal swells on the continents should be associated with rifting if they are more than about 1 km tall while thermal swells in the oceans never achieve a state of average extensional stress. Turcotte (1993) calculated the swell-push force associated with the major rises at Atla and Beta. Phillips (1990) extended this idea further by showing that this relationship also holds for certain simple models of dynamic support by mantle convection. Using both geoid and topography data, Banerdt (1986) and, more recently, Herrick and Phillips (1992) made assumptions about the depth and mode of compensation to compute the global stress pattern and mantle convection pattern, respectively. By constructing suites of models, these authors were able to match geoid height and topography over various features but were unable to arrive at a stress pattern that matches the geoid height over the entire planet. The major improvement of our model is that the depth and mode of compensation do not enter into the calculations and yet we match the geoid height over the entire planet. Indeed, the magnitude of the stress (integrated over the plate thickness) depends only on geoid height and well known parameters; the most poorly known parameter is Poisson's ratio.

SWELL-PUSH BODY FORCE IS THE GRADIENT OF THE GEOID

The most important aspect of the model is that the swell-push body force $\mathbf{f}(\mathbf{x})$, integrated through the thickness of the lithosphere L, is equal to the gradient of the geoid height ∇N. Only the horizontal components of the force vector are considered because we assume that local isostatic compensation prevails so the integrated vertical force is zero. To establish this relationship we initially assume all topography is locally compensated somewhere within the lithosphere although the mode and depth of compensation can vary laterally. The two-dimensional Fourier transform of the geoid height is

$$N(\mathbf{k}) = \frac{G}{g} \int_0^L \Delta\rho(\mathbf{k}) \frac{e^{-2\pi|\mathbf{k}|z}}{|\mathbf{k}|} \, dz, \qquad (1)$$

where $\Delta\rho$ is the density anomaly with respect to some reference density versus depth model (all stresses are relative to hydrostatic stresses in this reference density model), G is the gravitational constant, g is the average acceleration of gravity (8.87 m/s^2), $\mathbf{k} = (1/\lambda_x, 1/\lambda_y)$ is the two-dimensional wavenumber vector where λ is wavelength, and z is depth. In the long-wavelength limit $|\mathbf{k}|L \ll 1$, one can expand the exponential in a Taylor series and keep only the first two terms ($e^{-2\pi|\mathbf{k}|z} \cong 1 - 2\pi|\mathbf{k}|z$). Since a few areas have compensation depths of up to 300 km, the shortest wavelength that can be used is about 600 km which corresponds to a maximum spherical harmonic degree of 64; on the Earth, one can retain shorter wavelengths because average compensation depths are lower (Sandwell and MacKenzie 1989). The integral over the first term vanishes because the assumption of local isostasy. The familiar result is that the geoid height is the first moment of the density anomaly (Turcotte and Schubert 1982).

$$N = \frac{-2\pi G}{g} \int_0^L \Delta\rho(z)z \, dz \qquad (2)$$

A number of authors (Parsons and Richter 1980, Dahlen 1981, Fleitout and Froidevaux 1982, 1983) have shown that the swell-push force is also related to the first moment of
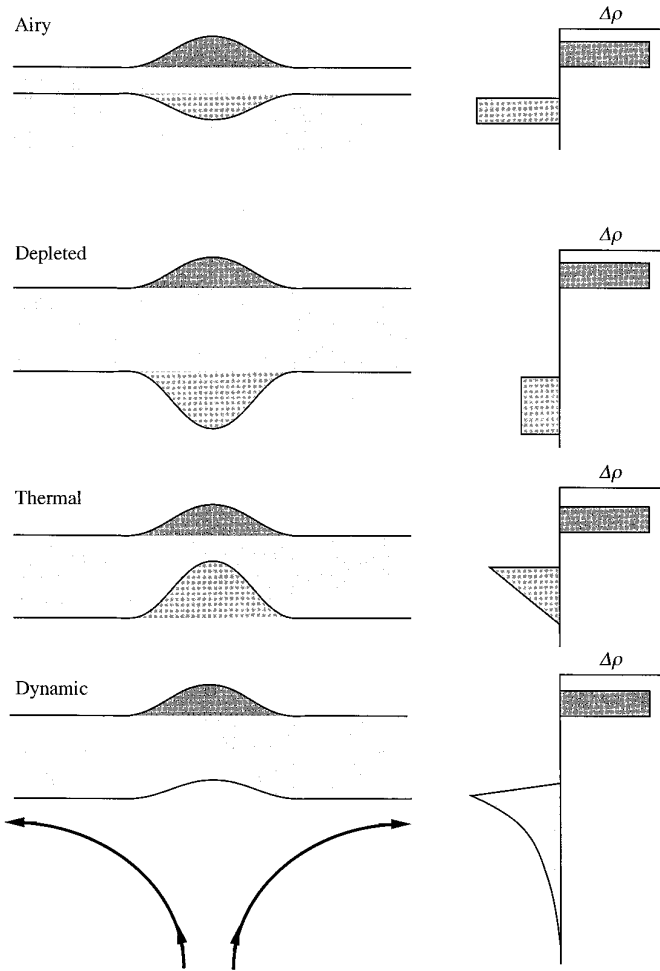
FIG. 1. Types of isostatic and dynamic compensation that result in a simple relationship between driving force and geoid height. All models assume that the wavelength of the topography exceeds both the flexural wavelength and the compensation depth. The top three models are all local isostatic models. The lower dynamic model assumes steady-state flow in a constant viscosity mantle (Phillips 1990).

the anomalous density (Fig. 1). The swell-push force F_s is equal to the vertical integral of the horizontal pressure gradient ΔP over the thickness of the lithosphere. Integration by parts provides two terms,

$$F_s = \int_0^L \Delta P(z)\, dz = [\Delta P(z)z]_0^L - \int_0^L z\, \frac{\partial\, \Delta P}{\partial z}\, dz. \quad (3)$$

The first term is zero because of isostasy (i.e., $\Delta P(L) = 0$). In the second term, the vertical derivative of the horizontal pressure gradient is related to the density anomaly $-g\, \Delta\rho(z)$ so the swell-push force is

$$F_s = g \int_0^L \Delta\rho(z) z\, dz. \quad (4)$$

From (2) and (4) the geoid and swell-push force are proportional to one another and the details of the compensation mechanism or compensation depth are irrelevant.

$$F_s = \frac{-g^2}{2\pi G}\, N \quad (5)$$

Dahlen (1981) shows that this relationship also results in the minimum deviatoric stress within the lithosphere needed to maintain the observed geoid. Phillips (1990) arrives at the same relationship (5) from a steady-state, isoviscous, dynamic model where topography is supported by shear traction along the base of the lithosphere. For the dynamic model there are geoid contributions from both the topography and the buoyant mantle below. While this infinite half space model is certainly too simple to reflect the actual dynamics of venusian convection, it suggests that there should be an approximate relationship between geoid height and lithospheric stress. The important conclusion is that for all of the compensation mechanisms shown in Fig. 1 (Airy or Pratt, depleted mantle, thermal, and dynamic) the swell-push force is proportional to the geoid height. The proportionality between lithospheric stresses and the geoid derived above holds to first order for non-isoviscous convection models, but over a more restricted wavelength band; relation (5) will be most accurate at short wavelengths and the degree to which our isostatic predictions for lithospheric stresses deviate from actual convective stresses will increase at long wavelengths. Geoid/topography admittance studies (e.g. Kiefer and Hager 1991, McKenize 1994, Phillips 1994, Simons *et al.* 1994, Smrekar 1994, Moresi and Parsons 1995, Simons *et al.* 1997) for Venus indicate that some highland regions such as Atla and Beta Regiones are supported by a combination of both dynamic and elastic compensation mechanisms. As we discuss later, our method may lead to an overestimate of lithospheric stresses in these regions; however, differences between our predictions and a possibly more realistic model incorporating convective and elastic stresses depend on many unknowns (e.g., viscosity structure as a function of depth, lithospheric rheology) and on our ability to generate realistic 3-D convection models. Given these caveats, the simple analytical approach presented here is appealing, and with a few additional assumptions one can calculate the stress in the venusian lithosphere directly from the geoid height, although this calculation will not provide insight into the support mechanism (static or dynamic) for topography on Venus.

The gradient of this swell-push force is a body force acting within the lithosphere. If the plate is thin compared to both the length scale of the geoid and the radius of Venus a (6051 km), then this body force is uniform

through the elastic lithosphere and it is tangential to the surface.

$$\mathbf{f}(\mathbf{x}) = \frac{-g^2}{2\pi G} \nabla N(\mathbf{x}) \qquad (6)$$

CARTESIAN SOLUTION

To illustrate how this body force is transmitted throughout the uppermost elastic layer of the lithosphere, consider the case of a thin elastic plate where the arbitrary vector body force is the gradient of a scalar function F_s. (The derivation is first done in Cartesian coordinates to expose the basic physical processes that are largely obscured by the more complicated mathematics of the spherical derivation.) Because the plate is thin, the vertical stress components integrated through the thickness of the plate are all zero.

$$\sigma_{zz} = \sigma_{xz} = \sigma_{yz} = 0 \qquad (7)$$

Note that these stresses have units of force per length. The equations of equilibrium are

$$\frac{\partial \sigma_{xx}}{\partial x} + \frac{\partial \sigma_{xy}}{\partial y} = 0$$

$$\frac{\partial \sigma_{xy}}{\partial x} + \frac{\partial \sigma_{yy}}{\partial y} = 0, \qquad (8)$$

where Goodier's method (Boley and Weiner 1960, p. 77) was used to remove the body forces from the equilibrium equations and insert them into the strain–stress relationship.

$$\varepsilon_{xx} = \frac{1}{E}\left[\sigma_{xx} - \nu\sigma_{yy} - (1 - 2\nu)F_s\right]$$

$$\varepsilon_{yy} = \frac{1}{E}\left[\sigma_{yy} - \nu\sigma_{xx} - (1 - 2\nu)F_s\right] \qquad (9)$$

$$\varepsilon_{xy} = \frac{1 + \nu}{E}\sigma_{xy}$$

The strains in (9) are integrated over the thickness of the lithosphere where E is Young's modulus (6.5×10^{10} kg m sec^{-2}) and ν is Poisson's ratio (0.25). This redefinition of the strain allows us to use an Airy stress function Φ to construct the components of stress.

$$\sigma_{xx} = \frac{\partial^2\Phi}{\partial y^2}, \quad \sigma_{xy} = -\frac{\partial^2\Phi}{\delta x \partial y}, \quad \sigma_{yy} = \frac{\partial^2\Phi}{\partial x^2} \qquad (10)$$

Insertion of (10) into (9) and then the equations of strain

compatibility results in the following fourth-order differential equation relating the Airy stress function to the swell-push force.

$$\nabla^4\Phi = (1 - 2\nu)\nabla^2 F_s \qquad (11)$$

The two-dimensional Fourier transform of (11) reduces this to an algebraic equation which is easily solved

$$\Phi(\mathbf{k}) = \frac{(1 - 2\nu)}{(2\pi|\mathbf{k}|)^2} \frac{g^2}{2\pi G} N(\mathbf{k}), \qquad (12)$$

where we have used Eq. (5) to show the explicit dependence on geoid height. Strains are calculated from the stress (with body force built-in) by inserting (12) into (10) and using the derivative property of the Fourier transform and then using Eq. (9).

$$\varepsilon_{xx}(\mathbf{k}) = \frac{k_x^2}{|\mathbf{k}|^2} \frac{(1 + \nu)(1 - 2\nu)g^2}{2\pi GE} N(\mathbf{k})$$

$$\varepsilon_{yy}(\mathbf{k}) = \frac{k_y^2}{|\mathbf{k}|^2} \frac{(1 + \nu)(1 - 2\nu)g^2}{2\pi GE} N(\mathbf{k}) \qquad (13)$$

$$\varepsilon_{xy}(\mathbf{k}) = \frac{k_x k_y}{|\mathbf{k}|^2} \frac{(1 + \nu)(1 - 2\nu)g^2}{2\pi GE} N(\mathbf{k})$$

These equations show the relationship between strain (positive in extension) and geoid height. Consider the principal strains ε_1 and ε_2,

$$\varepsilon_{1,2} = \frac{\varepsilon_{xx} + \varepsilon_{yy}}{2} \pm \left\{\frac{(\varepsilon_{xx} - \varepsilon_{yy})^2}{4} + \varepsilon_{xy}^2\right\}^{1/2}$$

$$\tan\alpha = \frac{2\varepsilon_{xy}}{\varepsilon_{xx} - \varepsilon_{yy}}, \qquad (14)$$

where α is the angle between ε_1 and the x-axis. Substitution of (13) into (14) reveals that the sum of the principal strains is equal to the geoid height scaled by the dimensionless constant $[(1 + \nu)(1 - 2\nu)g^2/2\pi GE = 1.8]$; positive geoid height causes average extension and negative geoid causes average compression. For example, the 120 m of geoid height over Atla and Beta will produce a vertically integrated strain of 216 m corresponding to a vertically integrated stress of 1.4×10^{13} Nt m^{-1} or an average stress of 280 MPa in a 50-km-thick elastic lithosphere. Note that the vertically integrated stress does not depend on Young's modulus. Later, when the calculations are done more precisely on a sphere, we arrive at almost the same values. Thus both the magnitude of the stress and the strain or stress pattern depend only on geoid height and there are no adjustable parameters.

In the more general case, one takes the two-dimensional

Fourier transform of the geoid, multiplies by the dimensionless constant, and divides by $|\mathbf{k}|^2$. At this point one can either multiply by the appropriate wavenumber (e.g., k_x^2 for ε_{xx}) and take the inverse Fourier transform or take the inverse transform first and then perform the derivatives in the space domain; the latter approach is more convenient when the calculations are done on a sphere.

SPHERICAL SOLUTION

A portion of the solution given in Banerdt (1986) is used for our calculation. The basic assumptions are that the tangential body force is poloidal (i.e., the gradient of the geoid) and there is no radial displacement of the lithosphere induced by the global stress pattern. Furthermore, bending moments or flexural components of stress are not considered. Banerdt (1986) defined a parameter $\Psi = 12a^2/h^2$ where a is the radius of Venus and h is the elastic thickness of the lithosphere. For an elastic thickness of less than 50 km (Johnson and Sandwell 1994), Ψ is very large; we take $1/\Psi = 0$ which simplifies the equations and leads to a solution that is similar in form to the Cartesian solution derived above.

The geoid height is first expanded (or provided) in spherical harmonic coefficients,

$$N(\theta, \phi) = \sum_{l=2}^{l_{max}} \sum_{m=-l}^{m=l} N_l^m Y_l^m(\theta, \phi), \qquad (15)$$

where Y_l^m are surface spherical harmonic functions of co-latitude θ and longitude ϕ (notation and normalization of Jackson (1975)). (See Masters and Shearer (1995) for the conversion from the geodesy convention for gravity coefficients into this convention.) Banerdt (1986) provided a relationship between the global strain field and a function $A(\theta, \phi)$,

$$\varepsilon_{\theta\theta} = \frac{\partial^2 A}{\partial \theta^2}$$

$$\varepsilon_{\phi\phi} = \frac{1}{\sin^2\theta}\frac{\partial^2 A}{\partial \theta^2} + \cot\theta\frac{\partial A}{\partial \theta} \qquad (16)$$

$$\varepsilon_{\theta\phi} = \frac{1}{\sin\theta}\left(\frac{\partial^2 A}{\partial\theta\partial\phi} - \cot\theta\frac{\partial A}{\partial\phi}\right).$$

Given the above assumptions and the approximation $1/\Psi = 0$, the spherical harmonic coefficients of A_l^m are related to the spherical harmonic coefficients of geoid height N_l^m.
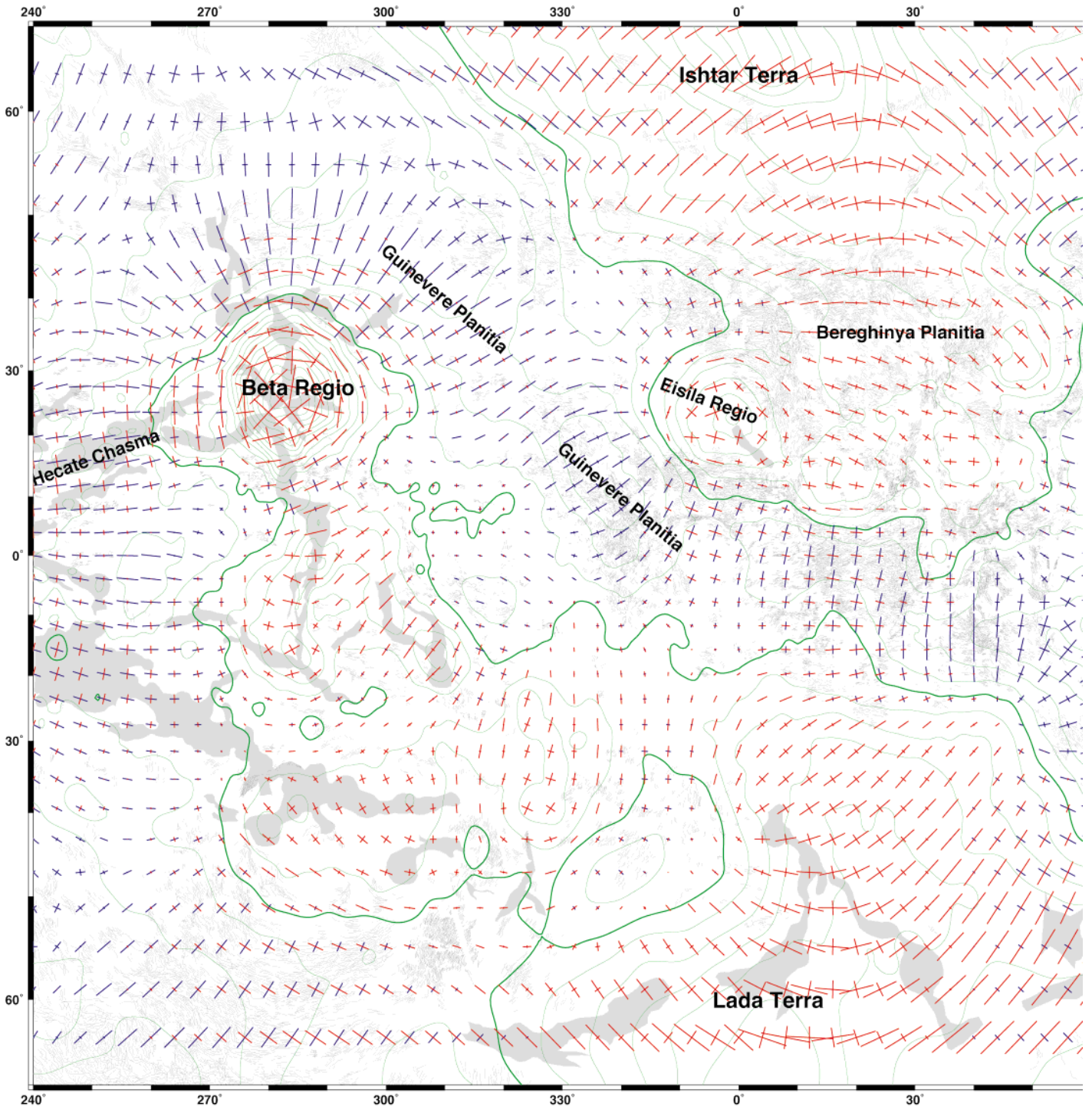
$$A_l^m = \frac{(1 + \nu)(1 - 2\nu)g^2}{2\pi GE} \frac{1}{l(l + 1) - 2} N_l^m \qquad (17)$$

Since Banerdt (1986) derived a similar equation by assuming a particular compensation depth and mechanism, our formula has a slightly different constant (i.e., the difference is $2/(1 - 2\nu)$). We arrived at this constant by forcing the spherical solution to match the Cartesian solution (12) for large spherical harmonic degree. Indeed the recipe for calculating strain from geoid height is the same in the spherical case as in the Cartesian case. First, the geoid height is expanded (or provided) in spherical harmonic coefficients (Konopliv and Sjogren 1994, 1996]. Then the A_{l^m} coefficients are computed using (17). This involves multiplication by a constant and scaling by a factor of about l^{-2} which is similar to the $|\mathbf{k}|^{-2}$ scaling used in Eqs. (12) and (13). Next the function $A(\theta, \phi)$ is calculated at many points on a sphere using the summations given in (15). Finally, the derivatives in (16) are evaluated using finite difference approximations.
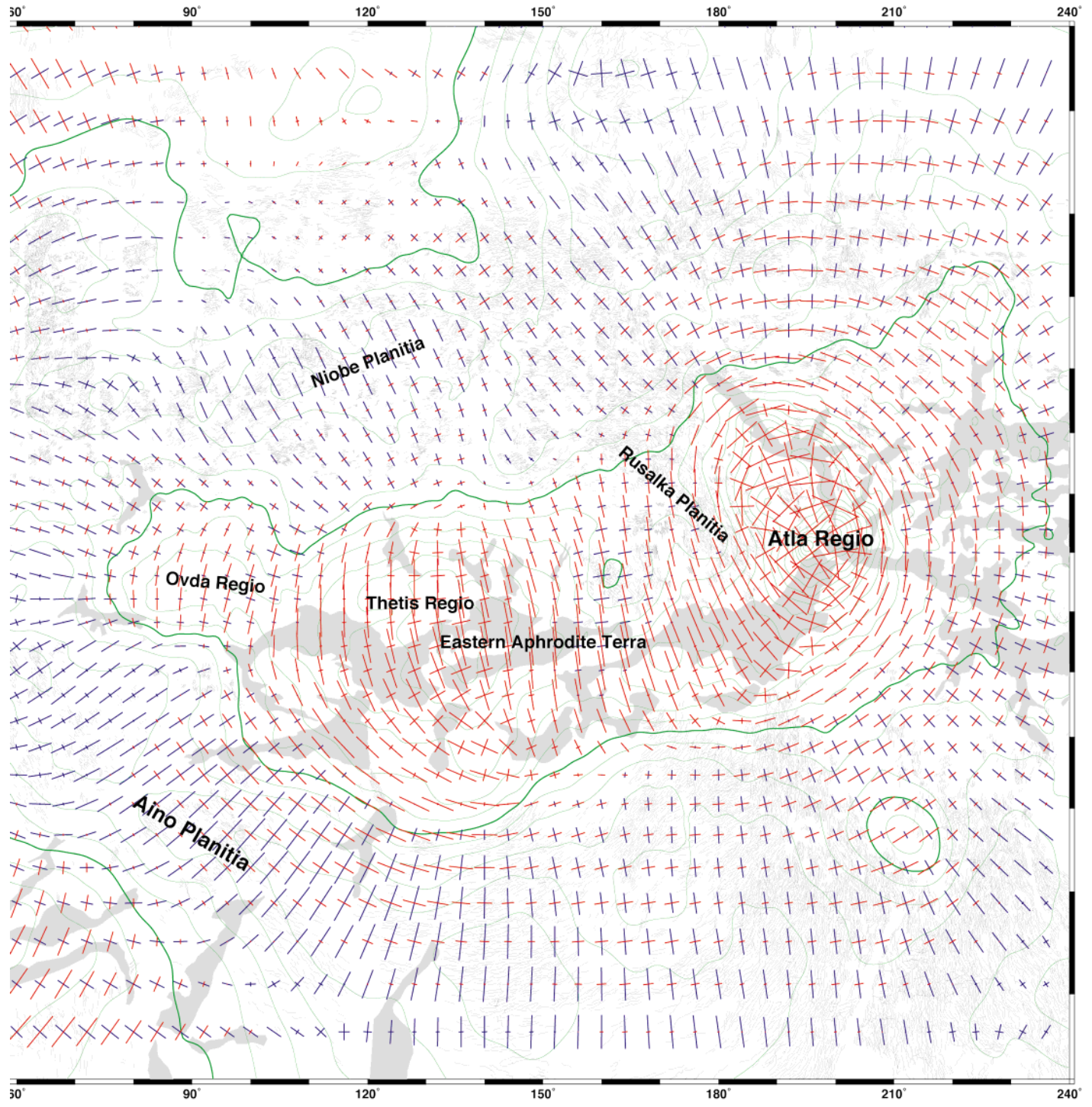
GLOBAL STRAIN AND STRESS FIELD

The principal horizontal components of the global strain field are shown in Fig. 2 (extensional strain, red; compressional strain, blue); contours of geoid height are also shown (green); principal stresses are approximately obtained by multiplying strain by Young's modulus so in fact the stresses are independent of Young's modulus. The geoid and strain model were calculated from the MGNP120LSAAP model (Konopliv and Sjogren 1996) to degree 120. An examination of the map shows that strain directions and relative magnitudes are predictable from the geoid height. Areas of positive geoid height show average extensional strain while areas of negative geoid height show compressional strain. The local curvature of the geoid governs the orientation of the principal strain. The rms magnitude sum of the principal stress is 5.9×10^{12} Nt m^{-1} (e.g., 117 MPa over a 50-km-thick lithosphere). The largest extensional stresses of 1.3×10^{13} Nt m^{-1} (e.g., 260 MPa in a 50-km-thick lithosphere) occur at the crests of Atla, Beta.

FIG. 2. Geoid height, model strain, wrinkle ridges, and rift zones for Venus. Geoid height is shown as green contours at 10 m intervals where 0 contour is thicker. Principal model strain times elastic lithospheric thickness (red, extension; blue, compression). For a 50-km-thick elastic plate, a strain of 0.0045 spans 10° of longitude which corresponds to stress of 292 MPa. Rift zones (Coburn 1993) are shown by gray areas and wrinkle ridges (Bilotti and Suppe 1995) are marked by thin black lines. Feature names are used in the text.

Niobe Planitia

Rusalka Planitia

Atla Regio

Ovda Regio

Thetis Regio

Eastern Aphrodite Terra

Aino Planitia

All of eastern Aphrodite and Ovda is characterized by roughly N–S extension and there is a broad area of extension around Lada Terra. The lowland plains, especially the large region south of Aphrodite, are characterized by large compressional strains.

FIRST-ORDER COMPARISON TO GEOLOGY

We now compare the model present-day strain to observed geologic structures that record past deformation. Since comparing strains predicted from an elastic model to observed fracture patterns is difficult and sometimes nonintuitive (Schultz and Zuber 1994), we will focus on the overall fracture patterns in relation to the sign of the model strain field. The most convincing correlation between the model and the observed deformation (Fig. 2) is that compressive deformation occurs in regions of low topography and geoid while extensional deformation is found primarily in highlands region with positive geoid. Wrinkle ridges, the most pervasive form of compressive deformation, are found primarily in areas of geoid less than 10 m and topography less than 6052 km planetary radius where the model predicts compression. The topographic distribution of rift zones is decidedly skewed toward high geoid (>10 m) and high elevation (>6052 km) (Price and Suppe 1995); the two major geoid highs of Venus correspond to Atla and Beta Regiones, which are the two major rift junctions on the planet. In fact, all of the major regions of high geoid and topography, with the exception of Ishtar Terra, show pervasive extensional collapse being the most recent tectonic deformation.

To perform a more detailed comparison of the model strain to this integrated deformation, we utilize GIS-based maps of rift zones (Coburn 1993) and wrinkle ridges (Bilotti and Suppe 1995) (Fig. 3). These maps were created from Magellan SAR images displayed at about 1 : 5 million and contain over 65,000 wrinkle ridges. When comparing geologic deformation signatures such as rifts with the model strain field one must remember that the deformation observed in the radar images represents the deformation integrated over the age of the surface while the model strain field is based entirely on the present-day geoid. The subset of rift zones that formed in the present-day stress field should have their rift axis perpendicular to the maximum extensional strain direction predicted by the model. Since wrinkle ridges are formed in compression, young wrinkle ridges will correspond to model shortening directions perpendicular to the regional strike of the structures.

COMPARISON WITH RIFT ZONES

As a class, rifts and chasmata are believed to be some of the youngest features on the planet based on the density of impact craters (Price and Suppe 1984), and so they
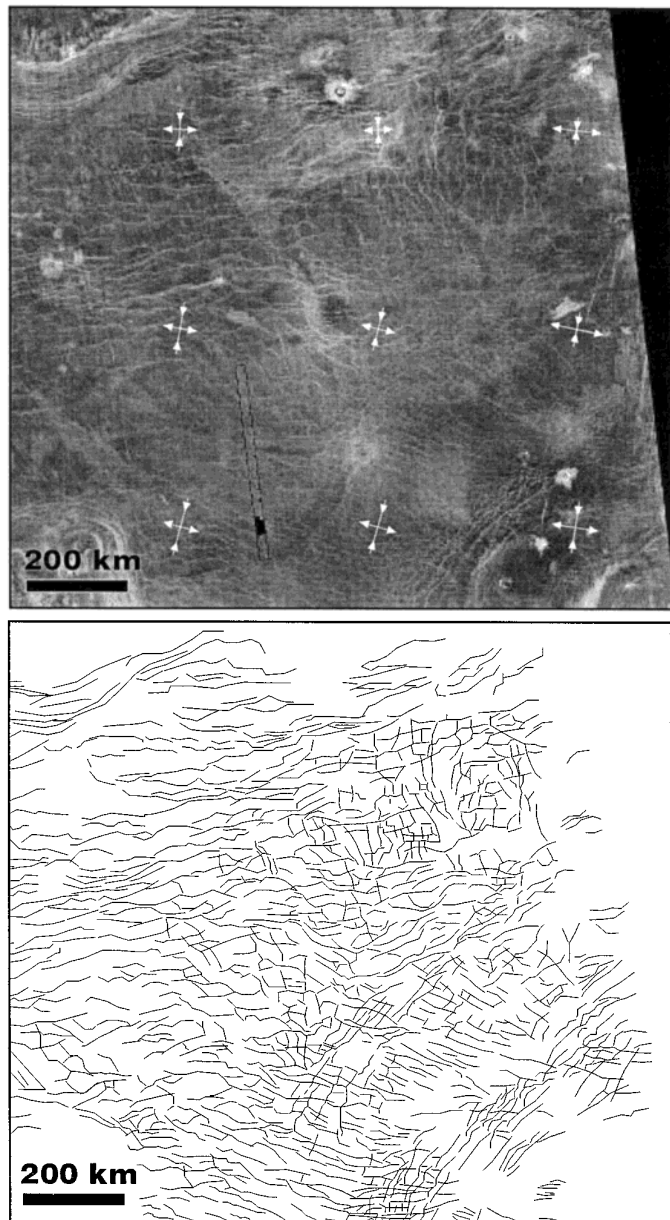

FIG. 3. SAR and mapped wrinkle ridges for an area centered on 0°N and 25°E. Wrinkle ridges were digitized at the uniform resolution offered by the Magellan C1-MIDRS. Arrows on the SAR image represent the predicted present-day strain predicted by the swell-push model; outward arrows represent extension and inward arrows represent compression.

provide some of the best candidates for comparing our model predictions with observed tectonic features. Rifts have a mean age of about 80–130 Myr relative to a global mean surface age of about 300 Myr (Price *et al.* 1996). The best correlation between present-day model strain and rift zones occurs at Atla, Beta and Eastern Aphrodite Terra (Senske *et al.* 1992).

Atla Regio contains three large volcanic edifices on the crests of the broad rise and five rift zones that radiate from the crest and terminate in the low-land areas. The model strains are greatest along the three most prominent rift zones; Ganis to the north, Parga to the east, and Dali Chasma which extends for several thousand kilometers to the southwest. Approximately N–S extensional strain is predicted in Eastern Aphrodite which is consistent with the hypothesis that some chasmata are caused by rifting (Hansen and Phillips 1993). The high correlation between rift patterns and model strain at Atla suggests that the rifts represent the most recent tectonic deformation episode in this area. Senske *et al.* (1992) showed that flows from the volcanic centers often overlay the rift zones which suggests they are the youngest volcanic features.

A similar high correlation between model strain and rift zones occurs at Beta Regio. Here the model predicts E–W extension along a N–S line running through the crest of Beta which correlates well with the location of Devana Chasma. In addition, the model predicts that moderate E–W extension continues along the same trend to 20°S which agrees with the continuation of the rift zone. N—S extension is predicted along Hecate Chasma although the zone of predicted extension extends only about half-way to the corona at 251.5°E, 16.0°N. Based on stratigraphic relationships, Senske *et al.* (1992) related the Hecate rift arm to an earlier extensional event which would suggest that the geoid anomaly associated with this earlier event has decayed. Hamilton and Stofan (1996) also interpreted Hecate Chasma to be associated with an extensional regime, with earlier broad diffuse extension having affected the region, followed by later concentration of strain into narrow zones resulting in formation of the chasmata.

Eistla Regio is also a major volcanic rise and geoid high. The predominant features of Eistla Regio, Sif and Gula Montes, are two major shield volcanoes. Both have extensive lava flows that postdate the heavily deformed plains to the south and northeast (Marchenko 1994) and are, along with the rift zone Guor Linea to the southeast, the youngest tectono-volcanic features in western Eistla. The model predicts that maximum extensional strains should occur beneath the volcanoes and continue to a lesser extent along Guor Linea, an isolated rift zone. Unlike Atla and Beta Regiones, rifting near Eistla Regio is isolated to a region 900 km long and about 175 km wide. The rift zones of the other major volcanic centers form a part of a nearly globe-encircling rift system (Schaber 1982, Suppe and Connors 1992).

The southeast rim of Artemis Corona, which may be the site of subduction (McKenzie *et al.* 1992, Sandwell and Schubert, 1992a,b) or underthrusting (Brown and Grimm 1995) lies in the transition zone between extensional and compressional stress (Fig. 2). If Artemis is a plate boundary then our basic assumption of a single-plate planet is locally invalid. Other corona where subduction has been proposed (Schubert and Sandwell 1995) are too small to be resolved in the degree 120 spherical harmonic gravity model. Moreover, our assumed relationship between swell push and geoid height is not valid when the horizontal extent of the structure is not much greater than the compensation depth. Thus the large-scale model should not be applied to regional features showing evidence for high strain (>5%) or plate boundaries; this may include Ishtar Terra and its arcuate boundaries which show evidence for compression (Hansen and Phillips 1995) rather than extension as predicted by our model.

Western Aphrodite Terra is composed of the tessera plateaus Ovda and Thetis Regiones. Both are sub-continent scale features that have been extensively deformed in compression followed perhaps by widespread tectonic collapse. This was followed by a large-scale plains formation volcanic episode (Saunders 1995). The youngest features are the closely spaced fracture systems/rift zones which cut both the tessera and the plains. The rift zones, however, are overlain by lavas and other tectono-volcanic features related to coronae and volcanoes which are probably associated with the process of rift creation. The tesserae of both Ovda and Thetis exhibit basin and dome terrain (Hansen and Willis 1996), dominated in places by extensional structures, although the age of formation of these extensional features is unknown. Our model predicts extensional strain throughout the highlands of Aphrodite Terra, particularly along the major rift zones that follow the southern border of the plateaus. The orientation of the model maximum extensional strain is near perpendicular to the axis of each of the major rift zones in this region (from 90° to 160°E).

COMPARISON WITH WRINKLE RIDGES

Wrinkle ridges are the surface expression of compressive anticlines and thrust faults that occur in the plains of Venus (e.g., Bilotti 1992, Watters 1992, McGill 1993). Wrinkle ridges that can be observed in Magellan SAR are typically a few kilometers in width and range from a few kilometers to several thousand kilometers in length (Fig. 3). Using C-1 MIDRS of Magellan SAR data which are available globally, Bilotti and Suppe (in preparation) digitized wrinkle ridges over most of the surface of Venus to achieve a uniform-coverage, global perspective. An example for an area at 0°N and 25°E is shown in Fig. 3. Based on the length of fold limbs and a fault–bend–fold model (Suppe 1983) for wrinkle ridge formation, Bilotti (1992) estimated that wrinkle ridges represent between 2 and 5% shortening regionally. This amount of deformation is not significant on a small scale, but wrinkle ridges form continuous patterns over the plains of the entire planet with inter-ridge

spacings that remain consistent over many thousands of kilometers.

In many places on Venus there are intersecting trends of wrinkle ridges that probably represent several generations of compressive deformation. Examples of this occur at ~340°E, 0°N, at the southern end of Guinevere Planitia and northeast of Eistla Regio in Bereghinya Planitia. These regions remind us that the folds and faults we map are a result of deformation integrated over the age of the surface. Because of their polydeformed nature, these regions need to be interpreted more rigorously than is possible in this paper. Direct comparison between wrinkle ridges and the model strains will therefore be limited to regions that have simpler strain patterns.

The most striking aspect of the distribution of wrinkle ridges on Venus is the continuous pattern surrounding southern Aphrodite Terra from 60°E in Aino Planitia to 200°E south of Dali Chasma. The orientation of the compressional strain predicted by the model agrees with the orientation of the wrinkle ridges between 60° to 150°E. However, between 150°E and 200°E, the wrinkle ridges turn to the north and the predicted shortening direction remains N–S. Since this trend of wrinkle ridges abruptly ends at the rift zones near Dali Chasma and then continues north of the rifts into Rusalka Planitia, we might speculate that this part of the wrinkle ridge trend predates the formation of the rifts and Atla Regio.

The predicted compressive strain orientation and wrinkle ridge deformation are in good agreement over Guinevere Planitia between 10° and 30°N. The mapped wrinkle ridges follow the elongate geoid depression that lies to the west of Eistla Regio as the model predicts. Wrinkle ridge density decreases greatly into central and northern Guinevere, closer to the volcanic rise of Beta Regio. In this region the plains units show more distinct flow morphology (Price 1995) and there is a greater abundance of coronae, both suggesting that the age of the plains here is relatively younger than to the south (Arvidson *et al.* 1992). This is probably due to the volcanism of Beta Regio. At the southern end of Guinevere, the above wrinkle ridge trend continues into a region with as many as four generations of compressive deformation while the predicted strain decreases.

In Niobe Planitia, to the north of Aphrodite Terra, the E–W trend of wrinkle ridges also agrees well with the predicted strain orientations. In this case, there is another N–S set of wrinkle ridges which is the older of the two sets. The N–S set is also more local, there are no other coherent sets of N–S wrinkle ridges for 20° in any direction. To the west of Niobe (near 20°N, 70°E), the predicted shortening directions bend to the south as does the main trend of wrinkle ridges. Also in this region we see other wrinkle ridge sets, several of which appear older than the main set. To the east of Niobe, in Rusalka Planitia, the

predicted compressive strain decreases, but the concentration of wrinkle ridges increases. This suggests that the wrinkle ridges of Rusalka Planitia are not present-day features.

The area of greatest disagreement between the model and the wrinkle ridge map is the Bereginya Planitia region. The model predicts that extension dominates in this region yet there is a high density of wrinkle ridges. This region is bounded to the south by the major volcanic edifices of Eistla Regio and Bell Regio. The region is dominated by large volcanic flows, coronae, and small tessera blocks (~10,000 km^2 scale). Many of the wrinkle ridges in this region are in and around the many coronae allowing the possibility that they formed due to local processes related to the formation or collapse of the coronae. The more simple interpretation is that the wrinkle ridges of this region are old features relative to the volcanism and uplift of this region.

ESTIMATES OF LITHOSPHERIC STRENGTH

Since the major highland rises, Atla, Beta, and Eastern Aphrodite, show evidence of rifting which is in agreement with the predictions of the model, one can compare the estimates of integrated stress to the integrated yield strength of the lithosphere for a variety of geotherms. We assume a 30-km-thick dry diabase crust (Grimm 1994, McKenzie 1994. Mackwell *et al.* 1995) and dry olivine mantle (Goetze and Evans 1979) and calculate yield strength versus depth for a variety of geotherms; 4 and 8 K/km are shown in Fig. 4a. The overall strength of the lithosphere in tension is the integral of yield strength over depth. This can be compared with the maximum extensional stress times the plate thickness at Atla, Beta, and Eastern Aphrodite which is 1.6×10^4 MPa km. Figure 4b shows this comparison for temperature gradients ranging from 2 to 16 K/km. Since these sites show evidence for rifting, this comparison provides a lower bound on the thermal gradient of 7 K/km which corresponds to an upper bound on elastic thickness of about 42 km and an upper bound on thermal lithospheric thickness of about 115 km. A thicker crust would decrease the integrated strength of the lithosphere which would require a decrease in the minimum temperature gradient while a thinner crust would have negligible effect on overall lithospheric strength. Note that this estimate of lithospheric, thickness (~115 km) corresponds to the crests of the major thermal swells. If these swells are primarily compensated by thinning of the lithosphere then the lithosphere away from the swells must be much thicker, perhaps 300 km (Kucinskas and Turcotte 1994, Moore and Schubert 1995). Alternatively, if these swells are primarily dynamically supported (McKenzie 1994, Simons *et al.* 1994), then it is likely that convective stresses will account for some of the long-wavelength ge-
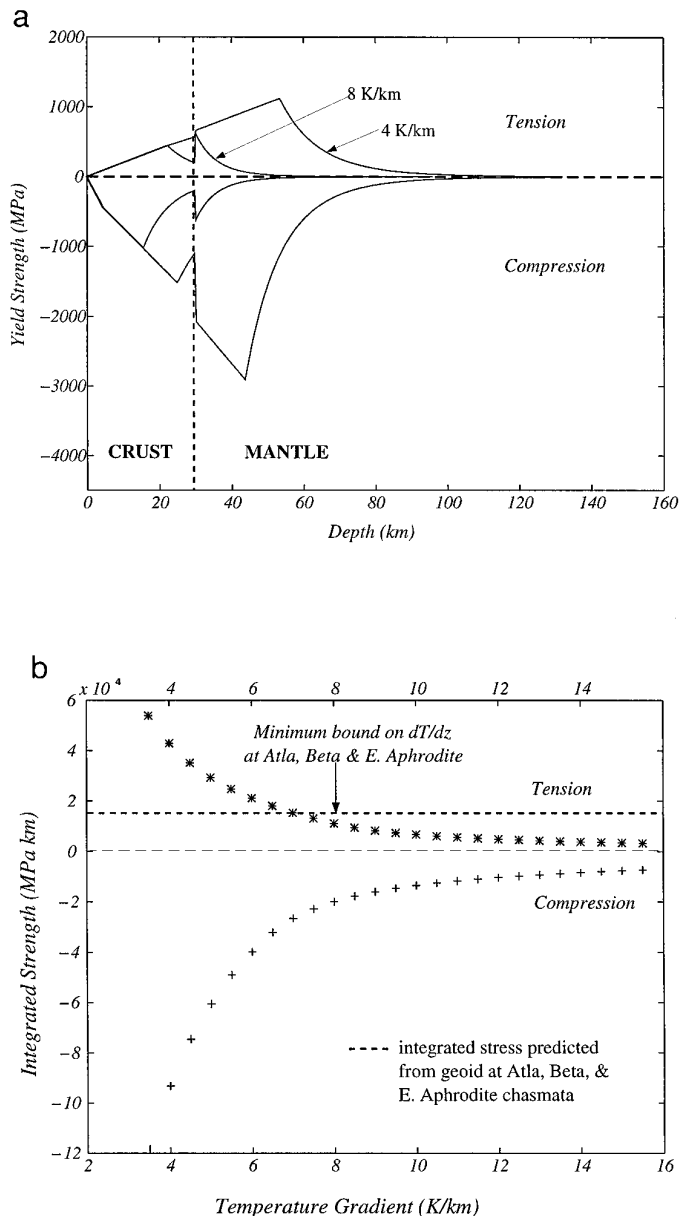
FIG. 4. (a) Yield strength versus depth for a dry olivine lithosphere (Goetze and Evans 1979) and 30-km-thick dry diabase crust (Mackwell *et al.* 1995) for geotherms of 4 and 8 K/km. The weaker crustal rheology has little effect on the overall strength of the lithosphere for a low thermal gradient. (b) Integrated yield strength in both tension and compression for thermal gradients ranging from 2 to 16 K/km. The lithosphere is about twice as strong in compression than it is in tension suggesting that rift zones represent complete lithospheric failure while wrinkle ridges represent elastic strain of the core of the lithosphere with brittle failure at the surface and ductile flow at depth. The horizontal dashed line is the integrated stress predicted by the model at the major geoid highs of 120 m.

oid, thereby reducing the amplitude of the geoid which needs to be explained by our model. If this is the case then our model may overestimate elastically supported stresses in the lithosphere and hence underestimate the lower bound on the thermal gradient in these regions. Also, in the case of dynamic support of the highland swells, the estimate of lithospheric thickness at the swells can apply to the whole planet. Thus our analysis adds little new information to the debate between static and dynamic support for these features.

CONCLUSIONS

Under the assumption that topography on Venus is locally compensated somewhere within the lithosphere or supported dynamically by poloidal flow in a nearly uniform viscosity mantle, we show that the swell-push body force acting on the lithosphere is proportional to the gradient of the geoid height. A second assumption that the lithosphere of Venus is well approximated by a uniform thickness elastic shell (i.e. no plate boundaries) is used to demonstrate that the magnitude swell-push force is proportional to geoid height, extensional stress over geoid highs, and compressional stress over geoid lows. This ratio depends only on well-known constants G, g, and ν. For example, at the crests of Atla and Beta where the geoid height is $\sim$120 m, the extension stress times the thickness is about 1.6×10^4 MPa km. The model also predicts that the direction of the principal stresses follow the local curvature of the geoid. Overall there is an excellent agreement between the strain predicted from geoid height and the strain inferred from rift zones and wrinkle ridges. Areas of disagreement or areas with orthogonal sets of wrinkle ridges can be used to sort out the changes in the driving forces over geologic time.

Since the venusian lithosphere shows evidence for failure in extension and compression, the imposed swell-push force is approaching the overall strength of the lithosphere. Yield strength envelope models predict that the lithosphere is about twice as strong in compression than it is in extension so our assumption of a uniform thickness elastic shell is obviously too simple. Moreover, the crests of the major swells are perhaps areas where the lithosphere is about 1/3 the thickness of the lithosphere in the plains. The implication is that much of the highland topography adjacent to the major rift zones is being maintained by large compressional stresses in the surrounding lowlands. These areas contain wrinkle ridges which reflect small compressional strains (2–5%) but not complete failure. A more detailed comparison of the predicted strains with the orientations and intensities of the wrinkle ridges may reveal areas where past stress patterns differ significantly from strains predicted from the present-day geoid.

ACKNOWLEDGMENTS

REFERENCES

Arvidson, R. E., M. C. Greeley, R. S. Malin, R. S. Saunders, N. Izenberg, J. J. Plaut, E. R. Stofan, and M. K. Shepard 1992. Surface modification of Venus as inferred from Magellan observations of plains. *J. Geophys. Res.* **97,** 13,303–13,318.

Banerdt, W. B. 1986. Support of long-wavelength loads on Venus and implications for internal structure, *J. Geophys. Res.* **91,** 403–419.

Bills, B. G., and F. G. Lemoine 1995. Gravitational and topographic isotropy of the Earth, Moon, Mars, and Venus, *J. Geophys. Res.* **100,** 26275–26295.

Bilotti, F., and J. Suppe 1992. Planetary distribution and nature of compressional deformation around Artemis Corona, Venus. *Lunar Planet. Sci. Conf.* Abstracts, XXIII.

Bilotti, F., and J. Suppe 1995. A global analysis of the distribution of wrinkle ridges on Venus, *EOS Trans. AGU* **74,** F333.

Boley, B., and J. H. Weiner 1960. *Theory of Thermal Stress.* Wiley, New York.

Brown, C. D., and R. E. Grimm 1995. Tectonics of Artemis Chasma: A venusian "plate" boundary, *Icarus* **117,** 219–249.

Brown, C. D., and R. E. Grimm 1996. Lithospheric rheology and flexure at Artemis Chasma, Venus. *J. Geophys. Res.* **101**(E5), 12,697–12,708.

Coburn, P. M. 1993. *Rifting on Venus: Observations from Stereo Imagery and Implications between Simple Rifts, Volcanic Rises, and Coronae on Venus.* B.A. thesis, Princeton University.

Crough, S. T. 1983. Rifts and swells: Geophysical constraints on causality. *Tectonophysics* **94,** 23–37.

Dahlen, F. A. 1981. Isostasy and the ambient state of stress in the oceanic lithosphere. *J. Geophys. Res.* **86,** 7801–7807.

Fleitout, L., and C. Froidevaux 1982. Tectonics and topography for a lithosphere containing density heterogeneities. *Tectonics* **1,** 21–56.

Fleitout, L., and C. Froidevaux 1983. Tectonic stresses in the lithosphere. *Tectonics* **2,** 315–324.

Goetze, C., and B. Evans 1979. Stress and temperature in the bending lithosphere as constrained by experimental rock mechanics. *Geophys. J. R. Astron. Soc.* **59,** 463–478.

Grimm, R. E. 1994. The deep structure of Venusian plateau highlands. *Icarus* **112,** 89–103.

Grosfils, E. B., and J. W. Head 1994. The global distribution of giant radiating dike swarms on Venus: Implications for the global stress state. *Geophys. Res. Lett.* **21,** 701–704.

Hamilton, V. E., and E. R. Stofan 1996. The geomorphology and evolution of Hecate Chasma, Venus. *Icarus* **121,** 171–194.

Hansen, V. L. and R. J. Phillips 1993. Tectonics and volcanism of eastern Aphrodite Terra, Venus: No subduction, no spreading. *Science* **260,** 526–530.

Hansen, V. L., and R. J. Phillips 1995. Formation of Ishtar Terra, Venus: Surface and gravity constraints. *Geology* **23**(N4), 292–296.

Hansen, V. L., and J. J. Willis 1996. Structural analysis of a sampling of tesserae: Implications for Venus geodynamics. *Icarus* **123,** 296–312.

Herrick, R. R., and R. J. Phillips 1992. Geological correlations with the interior density structure of Venus. *J. Geophys. Res.* **97,** 16017–16034.

Jackson, J. D. 1975. *Classical Electrodynamics.* Wiley, New York.

Johnson, C. L., and D. T. Sandwell 1994. Lithospheric flexure on Venus, *Geophys. J. Int.* **119,** 627–647.

Kiefer, W. S., and B. H. Hager 1991. A mantle plume model for the equatorial highlands of Venus. *J. Geophys. Res.* **96,** 20,947–20,966.

Konopliv, A. S., and W. L. Sjogren 1994. Venus spherical harmonic gravity model to degree and order 60. *Icarus* **112,** 42–54.

Konopliv, A. S., and W. L. Sjogren 1996. *Venus Gravity Handbook.* Technical Report 96–2, Jet Propulsion Laboratory, California Institute of Technology, Pasadena, California.

Kucinskas, A. B., and D. L. Turcotte 1994. Isostatic compensation of equatorial highlands on Venus. *Icarus* **112,** 104–116.

Mackwell, S. J., M. E. Zimmerman, D. L. Kohlsted, and D. S. Scherber 1995. Experimental deformation of dry Columbia diabase: Implications for tectonics on Venus. In Proc. of the 35th U.S. Symposium on Rock Mechanics (J. J. K. Daeman and R. A. Schultz, Eds.), pp. 207–214. Reno, Nevada.

Marchenko, A. G., 1994. Geologic mapping of the Sif Mons southern flank (preliminary results). In *Lunar Planet. Sci. Conf.* pp. 833–834. LPI, Houston, Texas.

Masters, T. G., and P. M. Shearer 1995. Seismic models of the Earth: Elastic and anelastic. In Global Earth Physics, Handbook of Physical Constants, AGU Reference Shelf 1. American Geophysical Union, Washington, DC.

McGill, G. E. 1993. Wrinkle ridges, stress domains, and kinematics of venusian plains. *Geophys. Res. Lett.* **20**(21), 2407–2410.

McKenzie, D. 1994. The relationship between topography and gravity on Earth and Venus. *Icarus* **112,** 55–88.

McKenzie, D., P. G. Ford, C. Johnson, B. Parsons, D. Sandwell, S. Saunders, and S. C. Solomon 1992. Features on Venus generated by plate boundary processes. *J. Geophys. Res.* **97,** 13,533–13,544.

Moore, W. B., and G. Schubert 1995. Lithospheric thickness and mantle/lithosphere density contrast beneath Beta Regio. *Venus* **22,** 429–432.

Moresi, L., and B. Parsons 1995. Interpreting gravity, geoid and topography for convection with temperature dependent viscosity: Application to surface features on Venus. *J. Geophys. Res.* **100,** 21,155–21,171.

Parsons, B., and F. M. Richter 1980. A relationship between the driving force and geoid anomaly associated with mid-ocean ridges. *Earth Planet. Sci. Lett.* **51,** 445–450.

Phillips, R. J. 1990. Convection-driven tectonics on Venus. *J. Geophys. Res.* **95,** 1301–1316.

Phillips, R. J. 1994. Estimating lithospheric properties at Atla Regio, Venus. *Icarus* **112,** 147–170.

Phillips, R. J., and K. Lambeck 1980. Gravity fields of the terrestrial planets. *Rev. Geophys.* **18,** 27–76.

Price, M. H. 1995. *Dating Resurfacing on Venus Using Impact Crater Densities from Gis-Based Global Mapping.* Ph.D. thesis, Princeton University, Princeton.

Price, M., and J. Suppe 1994. Mean age of rifting and volcanism on Venus deduced from impact crater densities. *Nature* **372,** 756–759.

Price, M., and J. Suppe 1995. Constraints on the resurfacing history of Venus from the hypsometry and distribution of volcanism, tectonism, and impact craters. *Earth, Moon, Planets* **71,** 99–145.

Price, M., G. Watson, C. Brankman, and J. Suppe 1996. Dating volcanism and rifting on Venus using impact crater densities. *J. Geophys. Res.* **101,** 4657–4671.

Sandwell, D. T., and K. R. MacKenzie 1989. Geoid height versus topography for oceanic plateaus and swells. *J. Geophys. Res.* **94,** 7403–7418.

Sandwell, D. T., and G. Schubert 1992a. Evidence for retrograde lithospheric subduction on Venus. *Science* **257,** 766–770.

Sandwell, D. T., and G. Schubert 1992b. Flexural ridges, trenches and outer rises around Venus coronae. *J. Geophys. Res.* **97,** 16,069–16,083.

Saunders, S. 1995. Ovda margin tectonic relationships. *EOS Trans. AGU* **76**(46), F242.

Schaber, G. G. 1982. Venus: Limited extension and volcanism along zones of lithospheric weakness. *Geophys. Res. Lett.* **9,** 499–502.

Schubert, G., and D. T. Sandwell 1995. A global survey of possible subduction sites on Venus. *Icarus* **117,** 173–196.

Schultz, R. A., and M. T. Zuber 1994. Observations, models, and mechanisms of failure of surface rocks surrounding planetary surface loads. *J. Geophys. Res.* **99,** 14,691–14,702.

Senske, D. A., G. G. Schaber, and E. R. Stofan 1992. Regional topographic rises on Venus: Geology of western Eisla Regio and comparison to Beta and Atla Regio. *J. Geophys. Res.* **97,** 13,395–13,420.

Simons, M., B. H. Hager, and S. C. Solomon 1994. Regional variations in the geoid/topography admittance of Venus. *Science* **264,** 798–803.

Simons, M., S. C. Solomon, and B. H. Hager 1997. Localization of gravity and topography: Constraints on the tectonics and mantle dynamics of Venus. *Geophys. J. Int.,* in press.

Sjogren, W. L., B. G. Bills, P. B. Birkeland, A. R. Esposito, N. A. Konopliv, S. J. Mottinger, S. J. Ritke, and R. J. Phillips 1983. Venus gravity anomalies and their correlations with topography. *J. Geophys. Res.* **88,** 1119–1128.

Smrekar, S. E. 1994. Evidence for active hotspots on Venus from analysis of Magellan gravity data. *Icarus* **112,** 2–26.

Smrekar, S. E., and R. J. Phillips 1991. Venusian highlands: Geoid to topography ratios and their implications. *Earth Planet. Sci. Lett.* **107,** 109–119.

Solomon, S. C. *et al.* 1992. Venus Tectonics: An overview of Magellan observations. *J. Geophys. Res.* **97,** 13,199–13,255.

Suppe, J. 1983. Geometry and kinematics of fault-bend folding. *Am. J. Sci.* **283,** 684–721.

Suppe, J., and C. Connors 1992. Linear mountain belts and related deformation on Venus. In *Lunar and Planetary Science Conference,* pp. 1389–1390. LPI, Houston, Texas.

Turcotte, D. L. 1993. An episodic hypothesis for venusian tectonics. *J. Geophys. Res.* **98,** 17,061–17,068.

Turcotte, D. L., and G. Schubert 1982. *GEODYNAMICS: Applications of Continuum Physics to Geological Problems.* Wiley, New York.

Watters, T. R. 1992. System of tectonic features common to Earth, Mars, and Venus. *Geology* (*Boulder*) **20**(7), 609–612.